# Observations of Seyferts by OSSE and parameters of their X-ray/gamma-ray sources


Andrzej A. Zdziarski
*N. Copernicus Astronomical Center, Bartycka 18, 00-716 Warsaw, Poland*
aaz@camk.edu.pl

Juri Poutanen
*Stockholm Observatory, SE-133 36 Saltsjöbaden, Sweden*
juri@astro.su.se
and

W. Neil Johnson
*E. O. Hulburt Center for Space Research, Naval Research Laboratory, Washington, DC 20375, USA*
johnson@osse.nrl.navy.mil


## ABSTRACT


We present a summary of spectra of Seyfert galaxies observed by the OSSE detector aboard *Compton Gamma Ray Observatory.* We obtain average spectra of Seyferts of type 1 and 2, and find they are well fitted by thermal Comptonization. We present detailed parameter ranges for the plasma temperature and the Compton parameter in the case of spherical and slab geometries. We find both the average and individual OSSE spectra of Seyfert 2s are significantly harder than those of Seyfert 1s, which difference can be due to anisotropy of Compton reflection and/or Thomson-thick absorption.



*Subject headings:* galaxies: active — galaxies: Seyferts — gamma rays: observations


## 1. Introduction

One of major unresolved problems of astrophysics of active galactic nuclei (AGNs) is the form of their soft $\gamma$-ray spectra (at energies $\gtrsim 100$ keV). The X-ray spectra of Seyfert galaxies are known relatively well, and consist (at $\gtrsim 2$ keV) of power-law, Compton reflection, and Fe K$\alpha$ components (e.g., Nandra & Pounds 1994; Nandra et al. 1997; Zdziarski, Lubiński & Smith 1999). However, the form of a high-energy cutoff of the power law remains poorly constrained. In the case of the brightest radio-quiet Seyfert, NGC 4151, results from the Oriented Scintillation Spectroscopy Experiment (OSSE; Johnson et al. 1993) aboard *Compton Gamma Ray Observatory* show the spectrum above 50 keV is well described by thermal Comptonization (e.g., Zdziarski, Johnson & Magdziarz 1996; Johnson et al. 1997a, hereafter J97). However, the X-ray spectrum of NGC 4151 is heavily absorbed and it is not clear whether its intrinsic spectrum is typical for Seyferts.

In the case of other radio-quiet Seyferts, constraints (from either OSSE, *RXTE* or *BeppoSAX*) on the form of their individual soft $\gamma$-ray spectra are rather poor due to limited photon statistics. One way to better constrain the soft $\gamma$-ray properties is to consider average spectra. Studies of the average $\sim$ 2–500 keV spectra of Seyferts observed by both *Ginga* and OSSE (Zdziarski et al. 1995; Gondek et al. 1996, hereafter G96) and *EXOSAT* and OSSE (G96) have shown that purely non-thermal models (e.g., Lightman & Zdziarski 1987) are highly unlikely. Although those authors have shown that thermal Comptonization provides a good description of the observed spectra, they have approximated model spectra from that process by a power law with an exponential cutoff. This simple model has also been used in numerous studies of individual objects (e.g., Zdziarski et al. 1994; Bassani et al. 1995; Weaver, Krolik & Pier 1998; Matt 1999; Perola et al. 1999), with the obtained e-folding energies being in fair agreement with those obtained for the average spectra. The e-folded power law, however, provides only a rough approximation to the actual spectral shape from thermal Comptonization, and the relationship between the e-folding energy and the electron temperature is not straightforward (e.g., Stern et al. 1995).

The purpose of this work is to determine the tightest currently possible constraints on the range of electron temperature, $kT$, and the Thomson optical depth, $\tau$, in radio-quiet Seyferts. To achieve this, we compute here the average OSSE spectra of *all* radio-quiet Seyfert 1s and of Seyfert 2s observed (except NGC 4151, the brightest object by far). We stress that OSSE still remains the most sensitive detector in the range $\gtrsim$ 100 keV currently operating and it will be surpassed only by the IBIS detector aboard *INTEGRAL* (Ubertini et al. 1999).

We fit the obtained data sets (with the useful energy range of $\sim$ 50–500 keV) with a highly-accurate model of thermal Comptonization of Poutanen & Svensson (1996). We find that their statistical accuracy is sufficient to provide useful constraints on the average parameters of the Comptonizing plasma in those sources. Furthermore, we apply this model to the previously obtained average OSSE spectrum of NGC 4151 (J97) and to the average $\sim$ 2–500 keV spectra of Seyfert 1s from *Ginga* and OSSE and *EXOSAT* and OSSE of G96.

## 2. The data

Table 1 gives the log of observations of all (except NGC 4151) radio-quiet Seyfert 1s and 2s detected by OSSE through the end of 1998. The data for individual objects include systematic errors estimated from the uncertainties in the low-energy calibration and response of the detectors using both in-orbit and pre-launch calibration data, and correspond to an uncertainty in the effective area in the OSSE response. This uncertainty is $\sim$ 3% at 50 keV decreasing to $\sim$ 0.3% at $\gtrsim$ 150 keV.

Table 1 also gives the photon power-law indices, $\Gamma$, fitted in the 50–200 keV range to sums of observations of individual Seyferts with detection significance $\gtrsim 4\sigma$. The indices are plotted in Figure 1. The mean and its error of the best-fit values for Seyfert 1s and 2s are $2.37 \pm 0.11$ and $2.06 \pm 0.15$, respectively. The mean weighted by the uncertainties and its error is $2.50 \pm 0.09$ and $2.05 \pm 0.09$, respectively. The intrinsic dispersions of the distributions (given by their standard deviations) are 0.37 and 0.42, respectively. The probability that the 2 distributions have the same mean and standard deviation is 5%, as obtained from the Student $t$ distribution.

We have then coadded the spectra of Seyfert 1s and 2s, obtaining data sets with $1.3 \times 10^7$ s and $9.1 \times 10^6$ s of OSSE exposure (scaled to a single OSSE detector with an effective area of 500 cm$^2$) with $2.8 \times 10^6$ and $2.7 \times 10^8$ of source photons (in the 50–150 keV range) from 17 and 10 AGNs, respectively. Source photons in the average Seyfert 1 and 2 spectra are then detected in the ranges of $\sim$ 50–500 keV and 50–400 keV, respectively. The upper limits at higher energies are much above our model spectra and thus we use only the above energy ranges in our fits.

## 3. Spectral fits to the average spectra

First, we note that the average OSSE data when fitted by a power law (PL) give spectral indices, $\Gamma$, significantly higher (Table 2) than the average X-ray spectral index of Seyfert 1s, $\Gamma_{\rm X} \simeq$ 1.9–2.0 (Nandra & Pounds 1994). This implies the presence of a spectral break between $\sim$ 20 and $\sim$ 50 keV. Then, we test for the presence of high-energy cutoffs in the average spectra themselves. We find statistically significant fit improvements when the power-law model is replaced by an e-folded power law (EPL) in both Seyfert 1s and 2s, see Table 2. The probability that the fit improvement were by chance (obtained using the F-test) equals to 0.003 in each case. This result argues strongly that spectra of individual Seyferts have high-energy cutoffs in a relatively narrow range of energies. If, in-

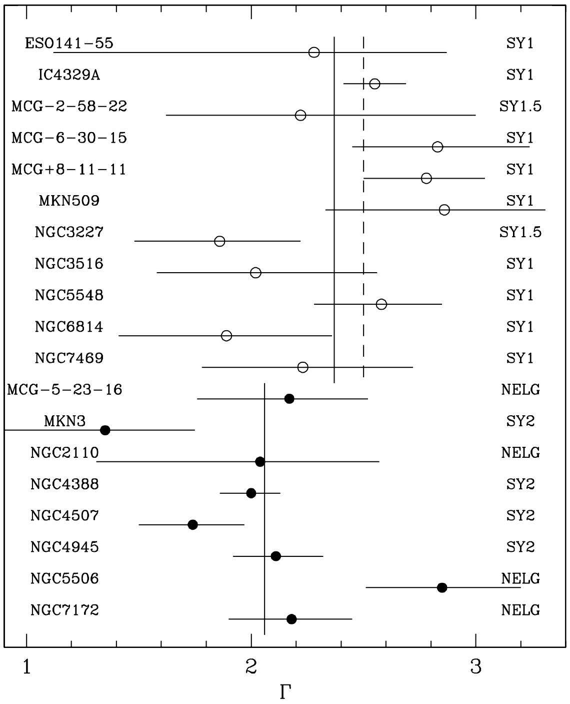


Fig. 1.— The distribution of 50–200 keV spectral indices in Seyfert 1s (open circles) and Seyfert 2s (filled circles). The upper vertical solid and dashed lines show the mean and weighted mean for Seyfert 1s, respectively, and the lower solid line corresponds to both means for Seyfert 2s. The error bars are $1\sigma$. The general classes of Seyfert 1 and 2 include those classified as Seyfert 1.5 and NELG (narrow emission-line galaxy), respectively, according to the NASA Extragalactic Database.

stead, there were a wide power-law distribution of the cutoff energies, the sum spectrum would be a power law without a cutoff.

We then consider a model with thermal Comptonization (TC) and Compton reflection. We use the model `compps` v3.4[1] (Poutanen & Svensson 1996) in XSPEC (Arnaud 1996). Since the actual geometry of Seyferts remains mostly unknown, we choose here spherical geometry, which is relatively generic, with spectra independent of the viewing angle. In similar spirit, we assume the source of seed photons at the center with a blackbody spectrum at $kT_{\rm bb} = 10$ eV. This model has been extensively tested against a Monte Carlo method (Gierliński 2000), and Figure 2 shows a good agreement between spectra obtained with the two methods (for the plasma parameters close to those of the *Ginga*-OSSE fit below). As the independent parameters of the model, we choose the electron temperature, $kT$, and the Compton $y$ parameter,

$$y \equiv 4\tau \frac{kT}{m_{\rm e}c^2}, \qquad (1)$$

where $\tau$ is the radial Thomson optical depth. A given value of $y$ corresponds to an approximately constant value of the 2–10 keV spectral index, $\Gamma_{\rm X}$ (e.g., Ghisellini & Haardt 1994; Poutanen 1998; Beloborodov 1999b; see below).

Reflection is treated using angle-dependent Green's functions of Magdziarz & Zdziarski (1995) and neglecting Comptonization of the reflected radiation in the hot plasma. Then, the obtained strength of reflection, $R$ (defined relative to the reflection strength from an isotropic point source above a slab), corresponds approximately to its unscattered fraction. Since the OSSE data cannot independently constrain $y$, $kT$ and $R$, we keep $R$ fixed at 0.75, obtained by fitting the average Seyfert-1 spectrum from *Ginga* and OSSE of G96. The inclination assumed by G96 is $\cos i = 0.87$ (e.g. Nandra et al. 1997), which we also assume in our fit to the Seyfert-1 spectrum. On the other hand, Seyfert 2s are most likely seen more edge-on, and we assume $\cos i = 0.4$ for the Seyfert-2 spectrum. We assume the reflecting medium is close to neutral with the abundances of Anders & Ebihara (1982).

[1]`compps` code is available on the internet at ftp://ftp.astro.su.se/pub/juri/XSPEC/COMPPS

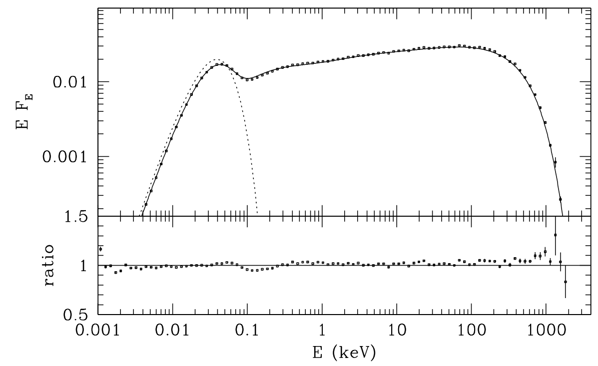


Fig. 2.— A comparison the thermal-Comptonization spectrum from `compps` (solid curve) with the corresponding one obtained using a Monte Carlo method (points with error bars). The lower panel shows the ratio between the latter and the former. The Comptonizing plasma forms a sphere with the electron temperature of $kT = 178$ keV and the radial optical depth of $\tau = 0.43$ with the source of blackbody seed photons at $kT_{\rm bb} = 10$ eV (dotted curve) at its center.

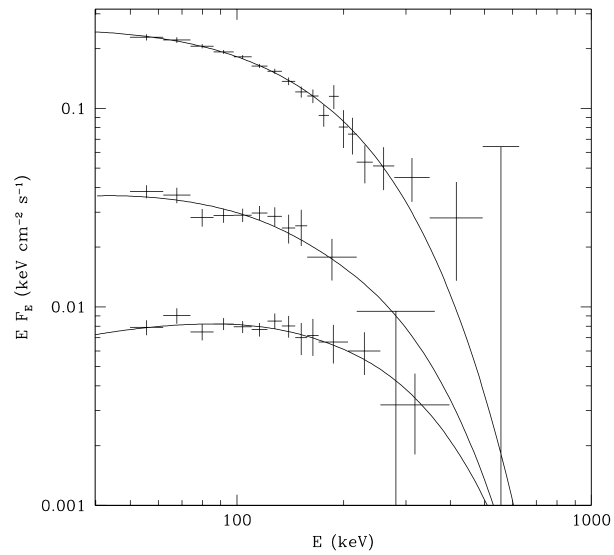


Fig. 3.— The average OSSE spectra of NGC 4151, Seyfert 1s and Seyfert 2s (rescaled by a factor 1/5), from top to bottom, fitted by thermal Comptonization in a spherical cloud and Compton reflection (with the assumed $R = 0.4$ and 0.75 for NGC 4151 and Seyferts, respectively).

The resulting data and model spectra are shown in Figure 3. The parameters are given in Table 2 and the error contours are shown in Figure 4. Its right vertical axis shows the value of the index $\Gamma_{\rm X}$ (of the Comptonization spectrum without the reflection component) computed at $kT = 100$ keV. As mentioned above, $\Gamma_{\rm X}$ is a weak function of $kT$ at a given $y$, and it changes within $\Delta\Gamma_{\rm X} \lesssim \pm 0.1$ for 50 keV $\lesssim kT \lesssim$ 200 keV.

We see that the error contour for Seyfert 1s is consistent within $1\sigma$ with their average X-ray spectral index being approximately $\Gamma_{\rm X} \simeq 1.9 \pm 0.1$ (Nandra & Pounds 1994; Zdziarski et al. 1999). The range of $kT$ corresponding to this $\Gamma_{\rm X}$ is $\sim$ 60–150 keV.

We have also refitted the average X-ray/$\gamma$-ray (X$\gamma$) spectra of Seyfert 1s observed by both *Ginga* and OSSE and by *EXOSAT* and OSSE of G96. We fitted them (in the range $\leq$ 500 keV) in the same way as in G96 except for modeling the primary continuum by thermal Comptonization instead of the e- folded power law. We obtain $kT$ = 190 keV, 166 keV, and $y$ = 0.57, 0.59, respectively, at the best fits, with the error contours shown in Figure 4. The resulting parameters are consistent within $1\sigma$ with those of the average spectrum of all Seyfert 1s observed by OSSE. However, our current data set, with photon statistics being much better than those of the two OSSE spectra of G96, represents the currently best estimate of the average $kT$ in Seyfert 1s.

Figures 3 and 4 also show the spectrum and the error contour, respectively, for the average of OSSE observations of the brightest Seyfert, NGC 4151 (J97) obtained with the same model. Since the strength of reflection in NGC 4151 is rather uncertain due to strong absorption in X-rays, we have constrained $R$ to be in the 0–1 range while computing the error contour (which assumption is responsible for its irregular shape). We see that the X-ray spectrum implied by these data is very similar to that of typical Seyfert 1s, with $\Gamma_{\rm X} \sim$ 1.8–2.0. The obtained range of temperature is relatively low, $kT \sim$ 50–80 keV, in agreement with the results of Zdziarski et al. (1996) and J97.

## 4. Comparison between Seyfert 1s and 2s

The weighted average of the 50–200 keV indices of individual objects (Table 1 and Figure 1) and the indices in the power-law fits to the sum spectra (Table 2) for Seyfert 1s, $2.50 \pm 0.09$ and $2.56 \pm 0.14$, respectively, are significantly softer than those for Seyfert 2s, $2.05 \pm 0.09$ and $2.21 \pm 0.12$. The probability that the 2 samples are drawn from the same distribution is only 5% (§2). This difference is confirmed by Figures 3, 4, where we see that the average spectrum of Seyfert 2s is noticeably harder than that of Seyfert 1s.

We have investigated whether this difference can be explained by the viewing angle different between Seyfert 1s and 2s. One relevant effect is the strength of Compton reflection decreasing with the increasing viewing angle. Since the spectrum from Compton reflection typically peaks around 30 keV followed by a steep decline at higher energies, the larger $R$ the softer the spectrum in the OSSE range. However, this effect is already included in our Comptonization/reflection model, and Figure 4 shows that it is not sufficient to account for the difference between the $y$ parameters of the average spectra. We note, however, that the average inclination of Seyfert 2s remains unknown. We have found we can fit the two spectra with the same Comptonization/reflection model (with $R = 0.75$) if $\cos i = 0^{+0.3}$ for Seyfert 2s within 90% confidence.

An additional subtle effect appears when the Comptonizing medium has a slab geometry. Namely, photons emitted at a large viewing angle (with respect to the slab normal) undergo a larger number of scatterings than those emitted at a small viewing angle, due to the escape probability at a given depth from the surface, $\tau'$, in a given direction being $\exp(-\tau'/\cos i)$. We have thus fitted our data with a model in which the Comptonizing medium forms a slab with a half-thickness $\tau$ and the seed photons are emitted by point sources in the midplane. We have first fitted with this model the *Ginga*-OSSE spectrum of G96, and then fixed the obtained $R$ in the fits to our average spectra. The resulting best-fit parameters are $kT = 63$ keV, 67 keV, $y = 0.34$, 0.48, for Seyfert 1s and 2s, respectively. The error contours are shown in Figure 5. We see that the two parameter ranges are still incompatible with each other. This means that the spectral shape does not change sufficiently due to this effect to account for the observed spectral difference (see Figure 3). For example, in the case of the best-fit Seyfert-1 model spectrum (including both Comptonization and reflection), the ratio of monochromatic fluxes at 150 keV and 50 keV increases only by 14% when the inclination changes from $\cos i = 0.87$ to $\cos i = 0.4$.

The above results also show that the obtained values of $kT$ and $\Gamma_{\rm X}$ only weakly depend on geometry. For Seyfert 2s, our results imply $\Gamma_{\rm X}$ between 1.4 and 1.9 and $kT$ between 50 and 170 keV.

We then consider possible effects of absorption/scattering in a torus surrounding the central source being important in Seyfert 2s. This can be an important effect in the OSSE range only when the torus is Thomson-thick, $N_{\rm H} \gtrsim 1.5 \times 10^{24}$ cm$^{-2}$. Then the hardening occurs (apart from a weak effect of photo-electric absorption) because the torus becomes more transparent to scattering with the increasing photon energy due to the Klein-Nishina effects. We have applied a numerical model of torus absorption/scattering of Krolik, Madau, & Życki (1994) to our average spectrum of Seyfert 2s assuming the intrinsic spectrum from thermal Comptonization of Seyfert 1s. We have obtained a good fit ($\chi^2_\nu = 22/26$) at $N_{\rm H} = 3 \times 10^{24}$ cm$^{-2}$ with an intrinsic TC spectrum identical in the cases of Seyfert 1s and 2s with a torus with an opening angle of 60°. However, since that numerical model does not allow for including Compton reflection from a disk, we cannot obtain meaningful constraints on its parameter space.

On the other hand, the only Seyfert 2 in our sample with a Thomson-thick absorber is NGC 4945 (Risaliti, Maiolino & Salvati 1999), with $N_{\rm H} \simeq 4 \times 10^{24}$ cm$^{-2}$ (see also Madejski et al. 2000), which nucleus is also viewed edge-on (Greenhill, Moran & Herrnstein 1997). Also, some effect of absorption on the OSSE band is possible in Mkn 3, with $N_{\rm H} \simeq 1.3 \times 10^{24}$ cm$^{-2}$ (Cappi et al. 1999). Then, $N_{\rm H} \sim (3\text{–}4) \times 10^{23}$ cm$^{-2}$ in NGC 4507 and NGC 4388, and $< 10^{23}$ cm$^{-2}$ in other Seyfert 2s in our sample (Risaliti et al. 1999), in which cases the effect of scattering on our spectra is negligible.

Thus, we cannot rule out an intrinsic difference between Seyfert 1s and 2s. Such a difference may be hinted for by X-ray spectra of individual Seyfert 2s often appearing harder than those of Seyfert 1s (e.g., Bassani et al. 1995; Smith & Done 1996). If indeed the X-ray spectra of Seyfert 2s were harder than those of Seyfert 1s, then our results above would indicate a correlation between the X-ray

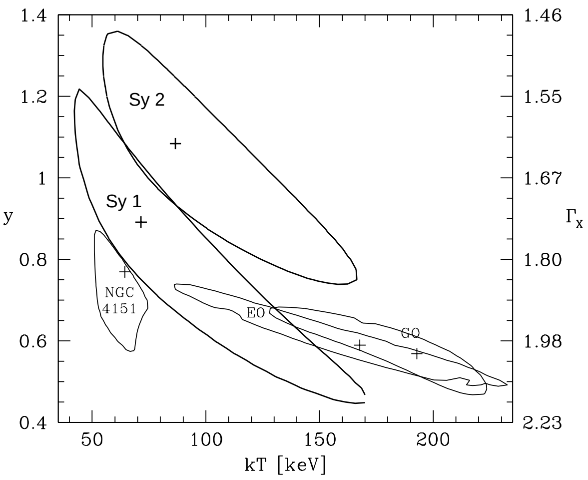


Fig. 4.— The $1\sigma$ error contours for the average OSSE spectra of Seyfert 1s and 2s fitted by thermal Comptonization in spherical geometry and Compton reflection. The contours for NGC 4151 and the average *Ginga*-OSSE (marked 'GO') and *EXOSAT*-OSSE (marked 'EO') spectra of G96 are also shown. The right vertical axes in this figure and Figure 5 give the 2–10 keV intrinsic spectral index for $kT = 100$ keV.

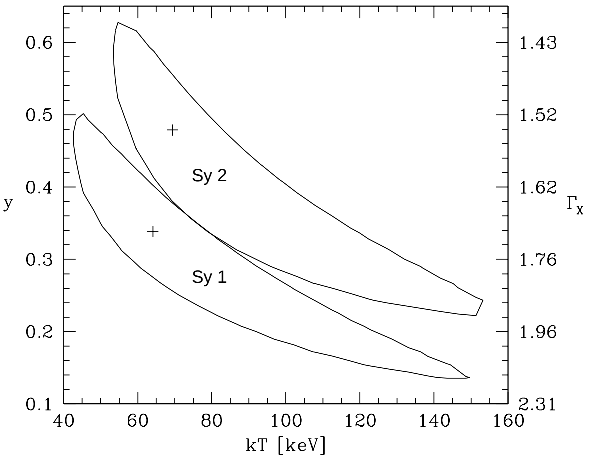


Fig. 5.— The $1\sigma$ error contours for the average OSSE spectra of Seyfert 1s and 2s in the case of thermal Comptonization in a slab.

slope and that in the OSSE band. On the other hand, we consider it possible that a complex structure of the absorber causes underestimating of the actual $\Gamma_X$ and $N_H$ in some Seyfert 2s.

Finally, we consider the possibility that our obtained difference between the soft $\gamma$-ray spectra of Seyfert 1s and 2s is simply caused by large relative contributions of a few bright objects to our average spectra. In the case of Seyfert 1s, 38% of the total number of source photons come from IC 4329A. For Seyfert 2s, we have 29% and 24% contributions from NGC 4388 and NGC 4945, respectively. Thus, if those objects had atypical spectra for their categories, they would significantly bias the shape of the average spectra. However, inspection of the distribution of the spectral indices in Figure 1 does not confirm this supposition. All 3 objects have spectra quite typical for their corresponding category.

On the other hand, it is interesting that 4 narrow-emission line galaxies (NELGs) in our sample of Seyfert 2s (Fig. 1) have somewhat softer spectra than regular Seyfert 2s (which effect is most pronounced for NGC 5506). NELGs are objects intermediate between Seyfert 1s and 2s, and are often considered together with Seyfert 1s in one class (e.g., Nandra & Pounds 1994). Figure 1 also marks 2 Seyferts classified as type 1.5 included in our Seyfert-1 sample.

In order to further investigate the issue of the effect of individual objects on our average spectra, we have also studied average Seyfert 1 and 2 spectra derived from observations up to the end of 1995. Those averages were based on $\sim 2/3$ of the statistics of the present spectra ($1.8 \times 10^6$ and $1.6 \times 10^6$ photons, respectively). Those samples contain, e.g., less than half of the photons from IC 4329A, none of NGC 3516, and almost none from NGC 4945 (see Table 1). Thus, if IC 4329A and NGC 4945 were substantially different from the average Seyfert 1 and 2, respectively, we would expect significant differences in the spectral shape of the old and new averages. However, the old and new average spectra can be fitted with identical models with hardly any increase of $\chi^2$ with respect to independent fits, and the F-test gives the probability that their spectral shape differ of $\lesssim 50\%$ for either Seyfert 1s or 2s.

Summarizing, we do find that Seyfert 2s have significantly harder spectra than Seyfert 1s (whereas their cutoff energies or temperatures are similar). This difference can be explained by the dependence of Compton reflection on orientation only for orientation close to edge-on ($\cos i \lesssim 0.3$). The angular dependence of thermal-Comptonization spectra in slab geometry is of relatively minor importance. The effect of Thomson-thick absorption in a torus surrounding the X$\gamma$ source is important in NGC 4945 and, possibly, Mkn 3.

## 5. Discussion

We have obtained quantitative constraints on the average electron temperature and the Compton parameter (or, equivalently, the Thomson optical depth) in Seyfert 1s and 2s (approximately $kT \sim 50$–$150\,\mathrm{keV}$ and $y < 1$, $\tau \lesssim 1$). These results put constraints on theoretical models of Seyferts as well as of the cosmic X$\gamma$ background. A detailed analysis of these constraints is beyond the scope of this work and we only outline the main relevant issues below.

Physically, the value of temperature in a source is determined by energy balance between heating and cooling. The balance depends, first of all, on the source geometry, which determines the flux of seed photons incident on the plasma. Production of seed photons appears to be dominated by blackbody photons emitted by an optically-thick medium in the vicinity of the hot plasma (Zdziarski et al. 1999), with the flux of thermal synchrotron photons being negligible in luminous AGNs (Wardziński & Zdziarski 2000). Thus, the values of $kT$ puts constraints on the geometry of the X-ray sources. Two geometries appear possible: a patchy corona above a cold accretion disk, and a hot accretion disk with an overlapping cold medium (either an outer cold disk, cold blobs or both, see, e.g., Poutanen 1998, Zdziarski et al. 1998).

The patchy corona geometry has been discussed recently by, e.g., Haardt, Maraschi & Ghisellini (1994), Stern et al. (1995), Poutanen & Svensson (1996), G96, and Beloborodov (1999a). In the case of Seyferts which have on average quite soft spectra ($\Gamma_X \sim 1.9$) and large reflection ($R \sim 0.75$), the patchy static corona still appears to be a viable model. The situation is different for those objects which have hard spectra and little reflection (see Zdziarski et al. 1999). In order to produce hard spectra, the emitting region should be well separated from the cold accretion disk (e.g., Svensson 1996), but in that case the predicted reflection is close to unity. Mildly relativistic motions of emitting plasma away from the disk, however, solve both problems producing hard spectra and little reflection (Beloborodov 1999a, b). We also note that this model can produce reflection larger than unity when emitting plasma is moving towards the disk.

Coronal models either with or without $e^{\pm}$ pair production are possible. We note that studies of thermal pair plasmas in pair equilibrium predict no distinct pair annihilation even from a pair-dominated plasmas (Maciołek-Niedźwiecki, Zdziarski & Coppi 1995). Thus, the lack of such a feature observed by OSSE (e.g., J97) does not rule out the presence of thermal $e^{\pm}$ pairs.

The hot disk model has been developed by Shapiro, Lightman & Eardley (1976), whose solution branch was cooling-dominated (and thermally unstable). Including advection gives rise to a stable, low-luminosity solution branch, and the intersection of the two branches limits the luminosity and the optical depth of an inner flow (Narayan & Yi 1995; Abramowicz et al. 1995; see Zdziarski 1998 for a model parametrizing the flow by $y$). The role of $e^{\pm}$ pair production is in general negligible (Björnsson et al. 1996). The values of $kT \sim 100$ keV and $\tau \lesssim 1$ are predicted by this model close to the maximum possible luminosity of the hot flow, in an agreement with our results. In order to account for the observed range of $\Gamma_X$ and $R$, an overlap between the hot disk and a cold one is required (Poutanen, Krolik & Ryde 1997; Zdziarski et al. 1999).

It is noteworthy that black-hole binaries in their hard states show X$\gamma$ spectra very similar to those of radio-quiet Seyferts. For example, spectra of Cyg X-1 and GX 339–4 have been well modeled by thermal Comptonization at $\tau \sim 1$, and $kT \sim 100$ keV and $\sim 60$ keV, respectively (Gierliński et al. 1997; Zdziarski et al. 1998). Hard-state X$\gamma$ spectra of X-ray novae are also similar (Grove et al. 1998).

Another class of objects for which a comparison with Seyferts is of interest is broad-line radio galaxies. Their X$\gamma$ spectra have been studied by Woźniak et al. (1998), who found both their X-ray and soft $\gamma$-ray spectra (with $\langle\Gamma_X\rangle = 1.67 \pm 0.18$, and $\langle\Gamma\rangle = 2.15 \pm 0.16$ in the 50–500 keV band) to be harder than those of Seyfert 1s (similarly to the case of Seyfert 2s). On the other hand, Woźniak et al. (1998) have not found a high-energy cutoff in their average OSSE spectrum, indicating the importance of non-thermal Compton scattering. This conclusion has to be considered tentative as the statistical accuracy of that spectrum is much below those of radio-quiet Seyferts. Still, a support for the importance of non-thermal processes in radio galaxies is provided by the $\gamma$-ray spectrum of the radio galaxy Cen A, which has a broken power-law form with the spectral breaks at $\sim 100$ keV and $\sim 10$ MeV (Steinle et al. 1998).

The form of the average spectra of Seyfert 1s and 2s is of primary importance synthesizing the cosmic X$\gamma$ background from individual sources. This synthesis appears possible provided Seyfert 2s dominate the hard X-ray background (e.g., Zdziarski et al. 1995; Comastri et al. 1995).

## 6. Conclusions

We have obtained error contours in the $kT$-$y$ space for the average spectra of Seyfert 1s and 2s observed by OSSE. Combining the contours for Seyfert 1s with their average X-ray spectral index of $\Gamma_X \simeq 1.9$–2 (Nandra & Pounds 1994), we obtain $kT \simeq 50$–150 keV. The corresponding Thomson optical depth ($\tau \simeq y 128\,\mathrm{keV}/kT$) of Seyfert 1s is $\tau \simeq 0.3$–1.5 in spherical geometry and $\tau \simeq 0.1$–0.6 in slab geometry.

We also find both the average and individual Seyfert-2 spectra are significantly harder than those of Seyfert 1s. This difference can be partly due to the spectral component from Compton reflection being weak in Seyfert 2s, provided their average inclination is edge-on enough. Furthermore, Thomson-thick absorption can account for the difference in 2 (out of 8) objects in our sample.

This research has been supported in part by the KBN grants 2P03C00511p0(1,4) and 2P03D00614, NASA grants and contracts, the Swedish Natural Science Research Council, and the Anna-Greta and Holger Crafoord Fund. We thank Marek Gierliński for his assistance with implementing models into the XSPEC software package and with Monte Carlo calculations, Piotr Życki for providing his Thomson-thick torus model, and the referee for insightful remarks.

## REFERENCES

Abramowicz, M. A., Chen, X., Kato, S., Lasota, J.-P., & Regev, O. 1995, ApJ, 438, L37

Anders, E., & Ebihara, M. 1982, Geochim. Cosmochim. Acta, 46, 2363

Arnaud, K. A. 1996, in ASP Conf. Series 101, Astronomical Data Analysis Software and Systems V, ed. G. H. Jacoby & J. Barnes (San Francisco: ASP), 17

Bassani, L., Malaguti, G., Jourdain, E., Roques, J. P., & Johnson, W. N. 1995, ApJ, 444, L73

Beloborodov, A. M. 1999a, ApJ, 510, L123

Beloborodov, A. M. 1999b, in ASP Conf. Series 161, High Energy Processes in Accreting Black Holes, ed. J. Poutanen & R. Svensson (San Francisco: ASP), 295

Björnsson, G., Abramowicz, M. A., Chen, X., & Lasota, J.-P. 1996, ApJ, 467, 99

Cappi, M., et al. 1999, A&A, 344, 857

Comastri, A., Setti, G., Zamorani, G., & Hasinger, G. 1995, A&A, 296, 1

Gierliński, M. 2000, PhD thesis, N. Copernicus Astron. Center, Warsaw

Gierliński, M., Zdziarski, A. A., Done, C., Johnson, W. N., Ebisawa, K., Ueda, Y., Haardt, F., & Phlips, B. F. 1997, MNRAS, 288, 958

Ghisellini, G., & Haardt, F. 1994, ApJ, 429, L53

Gondek, D., Zdziarski, A. A., Johnson, W. N., George, I. M., McNaron-Brown, K., Magdziarz, P., Smith, D., & Gruber, D. E. 1996, MNRAS, 282, 646 (G96)

Greenhill, L. J., Moran, J. M., & Herrnstein, J. R. 1997, ApJ, 481, L23

Grove, J. E., Johnson, W. N., Kroeger, R. A., McNaron-Brown, K., & Skibo, J. G. 1998, ApJ, 500, 899

Haardt, F., Maraschi, L., & Ghisellini, G. 1994, ApJ, 432, L95

Johnson, W. N., et al. 1993, ApJS, 86, 693

Johnson, W. N., McNaron-Brown, K., Kurfess, J. D., Zdziarski, A. A., Magdziarz, P., & Gehrels, N. 1997a, ApJ, 482, 173 (J97)

Krolik, J. H., Madau P., Życki, P. T. 1994, ApJ, 420, 57

Lightman, A. P., & Zdziarski, A. A. 1987, ApJ, 319, 643

Maciołek-Niedźwiecki, A., Zdziarski, A. A., & Coppi, P. S. 1995, MNRAS, 276, 273

Madejski, G. M., Życki, P. T., Done, C., Valinia, A., Blanco, P., Rothschild, R., & Turek, B. 2000, ApJ, in press

Magdziarz, P., & Zdziarski, A. A. 1995, MNRAS, 273, 837

Matt, G. 1999, in ASP Conf. Series 161, High Energy Processes in Accreting Black Holes, ed. J. Poutanen & R. Svensson (San Francisco: ASP), 149
Nandra, K., & Pounds, K. A. 1994, MNRAS, 268, 405
Nandra, K., George, I. M., Mushotzky, R. F., Turner, T. J., & Yaqoob, T. 1997, ApJ, 477, 602
Narayan, R., & Yi, I. 1995, ApJ, 452, 710
Perola, G. C., et al. 1999, A&A, 351, 937
Poutanen, J. 1998, in Theory of Black Hole Accretion Discs, ed. M. A. Abramowicz, G. Björnsson, & J. E. Pringle (Cambridge: Cambridge University Press), 100
Poutanen, J., & Svensson, R. 1996, ApJ, 470, 249
Poutanen, J., Krolik, J. H., & Ryde, F. 1997, MNRAS, 292, L21
Risaliti, G., Maiolino, R., & Salvati, M. 1999, ApJ, 522, 157
Shapiro, S. L., Lightman, A. P., & Eardley, D. M. 1976, ApJ, 204, 187
Smith, D. A., & Done, C. 1996, MNRAS, 280, 355
Steinle, H., et al. 1998, A&A, 330, 97
Stern, B. E., Poutanen, J., Svensson, R., Sikora, M., & Begelman, M. C. 1995, ApJ, 449, L13
Svensson, R. 1996, A&AS, 120C, 475
Ubertini, P., et al. 1999, Astr. Lett. Comm., 38, 799
Wardziński, G., & Zdziarski, A. A. 2000, MNRAS, 314, 183
Weaver, K. A., & Krolik, J. H., & Pier, E. A. 1998, ApJ, 498, 213
Woźniak, P. R., Zdziarski, A. A., Smith, D., Madejski, G. M., & Johnson, W. N. 1998, MNRAS, 299, 449
Zdziarski, A. A. 1998, MNRAS, 296, L51
Zdziarski, A. A., Fabian, A. C., Nandra, K., Celotti, A., Rees, M. J., Done, C., Coppi, P. S., & Madejski, G. M. 1994, MNRAS, 269, L55
Zdziarski, A. A., Johnson, W. N., Done, C., Smith, D., & McNaron-Brown, K. 1995, ApJ, 438, L63
Zdziarski, A. A., Johnson, W. N., & Magdziarz, P. 1996, MNRAS, 283, 193
Zdziarski, A. A., Poutanen, J., Mikołajewska, J., Gierliński, M., Ebisawa, K., & Johnson, W. N. 1998, MNRAS, 301, 435
Zdziarski, A. A., Lubiński, P., & Smith, D. A. 1999, MNRAS, 303, L11

This 2-column preprint was prepared with the AAS LATEX macros v5.0.

Table 1
OSSE observations of Seyferts[a]

| Object | $\Gamma^{b}$ or Dates | Exposure[c] | Photon flux[d] |
| --- | --- | --- | --- |
| | | | |
| | Seyfert 1s | | |
| ESO 141–55 | $2.28^{+0.59}_{-1.16}$ | 3.10 | $2.63 \pm 0.79$ |
| | 92/220–92/223 | 0.90 | $3.57 \pm 1.42$ |
| | 92/241–92/245 | 1.03 | $3.07 \pm 1.35$ |
| | 92/290–92/303 | 1.17 | $1.53 \pm 1.31$ |
| IC 4329A | $2.55^{+0.14}_{-0.14}$ | 27.44 | $7.74 \pm 0.40$ |
| | 92/283–92/289 | 1.10 | $7.35 \pm 1.64$ |
| | 92/309–92/322 | 2.77 | $7.93 \pm 1.01$ |
| | 93/013–93/033 | 4.17 | $8.93 \pm 0.66$ |
| | 94/305–94/313 | 1.08 | $3.64 \pm 2.78$ |
| | 95/024–95/045 | 4.13 | $6.93 \pm 0.96$ |
| | 96/212–96/226 | 2.52 | $6.85 \pm 1.24$ |
| | 96/226–96/233 | 1.40 | $6.94 \pm 1.65$ |
| | 96/233–96/240 | 1.67 | $7.52 \pm 1.52$ |
| | 96/303–96/317 | 2.93 | $11.61 \pm 1.00$ |
| | 97/217–97/230 | 5.68 | $6.85 \pm 1.20$ |
| III Zw II | — | 4.17 | $1.63 \pm 0.79$ |
| | 93/083–93/088 | 0.61 | $< 3.21$ |
| | 96/065–96/078 | 3.57 | $1.97 \pm 0.88$ |
| MCG –2-58-22 | $2.22^{+0.78}_{-0.60}$ | 2.95 | $3.72 \pm 0.88$ |
| | 93/053–93/056 | 0.59 | $< 3.40$ |
| | 93/088–93/091 | 0.43 | $2.86 \pm 2.11$ |
| | 93/125–93/126 | 0.38 | $3.94 \pm 2.11$ |
| | 95/094–95/101 | 1.55 | $5.27 \pm 1.32$ |
| MCG –6-30-15 | $2.83^{+0.41}_{-0.38}$ | 5.07 | $4.58 \pm 0.67$ |
| | 92/283–92/289 | 1.11 | $3.91 \pm 1.15$ |
| | 92/309–92/322 | 2.75 | $4.80 \pm 0.71$ |
| | 95/164–95/171 | 1.21 | $4.68 \pm 2.04$ |
| MCG +8-11-11 | $2.78^{+0.26}_{-0.28}$ | 14.61 | $4.13 \pm 0.39$ |
| | 92/163–92/177 | 6.70 | $4.41 \pm 0.51$ |
| | 93/145–93/151 | 1.94 | $2.50 \pm 0.94$ |
| | 95/234–95/250 | 5.97 | $4.33 \pm 0.68$ |
| Mkn 279 | — | 5.70 | $1.57 \pm 0.58$ |
| | 92/066–92/079 | 4.14 | $2.47 \pm 0.66$ |
| | 93/230–93/236 | 1.56 | $< 2.35$ |
| Mkn 509 | $2.86^{+0.45}_{-0.53}$ | 4.88 | $3.98 \pm 0.70$ |
| | 92/304–92/308 | 1.04 | $4.22 \pm 1.12$ |
| | 93/082–93/088 | 0.97 | $3.30 \pm 1.37$ |
| | 94/138–94/144 | 0.10 | $< 21.76$ |
| | 95/010–95/024 | 2.77 | $3.98 \pm 0.98$ |

TABLE 1—*Continued*

| Object | $\Gamma^{b}$ or Dates | Exposure[c] | Photon flux[d] |
|---|---|---|---|
| Mkn 841 | — | 2.64 | $3.56 \pm 1.02$ |
| | 92/108–92/114 | 0.26 | $< 5.15$ |
| | 96/277–96/289 | 2.38 | $3.79 \pm 1.09$ |
| NGC 3227 | $1.86^{+0.36}_{-0.38}$ | 10.97 | $3.40 \pm 0.55$ |
| | 95/003–95/010 | 0.40 | $4.09 \pm 3.03$ |
| | 95/220–95/234 | 2.42 | $3.09 \pm 1.49$ |
| | 95/234–95/250 | 5.90 | $2.84 \pm 0.67$ |
| | 95/290–95/304 | 2.25 | $5.08 \pm 1.10$ |
| NGC 3516 | $2.02^{+0.56}_{-0.44}$ | 10.50 | $2.97 \pm 0.64$ |
| | 97/175–97/195 | 5.07 | $2.38 \pm 0.88$ |
| | 97/245–97/252 | 1.64 | $5.15 \pm 1.67$ |
| | 97/266–97/280 | 3.12 | $2.67 \pm 1.18$ |
| | 98/013–98/021 | 0.67 | $3.45 \pm 2.92$ |
| NGC 3783 | — | 0.98 | $4.42 \pm 1.38$ |
| | 92/178–92/184 | 0.98 | $4.42 \pm 1.38$ |
| NGC 526A | — | 3.44 | $3.69 \pm 0.91$ |
| | 96/065–96/078 | 3.44 | $3.69 \pm 0.91$ |
| NGC 5548 | $2.58^{+0.27}_{-0.30}$ | 11.15 | $5.10 \pm 0.54$ |
| | 91/228–91/234 | 1.82 | $4.24 \pm 1.22$ |
| | 91/291–91/303 | 0.57 | $5.04 \pm 1.94$ |
| | 91/305–91/310 | 0.67 | $6.73 \pm 2.14$ |
| | 93/250–93/252 | 0.53 | $5.88 \pm 1.89$ |
| | 93/264–93/265 | 0.11 | $4.97 \pm 4.03$ |
| | 93/265–93/274 | 1.58 | $4.42 \pm 1.13$ |
| | 93/291–93/292 | 0.55 | $8.85 \pm 1.98$ |
| | 95/270–95/276 | 1.07 | $4.56 \pm 1.36$ |
| | 95/311–95/318 | 1.58 | $5.51 \pm 2.07$ |
| | 96/081–96/094 | 2.68 | $4.74 \pm 1.13$ |
| NGC 6814 | $1.89^{+0.47}_{-0.48}$ | 5.05 | $3.01 \pm 0.58$ |
| | 93/033–93/040 | 2.54 | $3.15 \pm 0.82$ |
| | 93/215–93/222 | 2.52 | $2.88 \pm 0.83$ |
| NGC 7213 | — | 5.15 | $2.12 \pm 0.86$ |
| | 93/328–93/335 | 0.90 | $< 3.81$ |
| | 94/032–94/039 | 0.47 | $5.13 \pm 2.99$ |
| | 95/010–95/024 | 2.14 | $3.52 \pm 1.15$ |
| | 96/205–96/212 | 1.64 | $3.35 \pm 1.78$ |
| NGC 7469 | $2.23^{+0.49}_{-0.45}$ | 9.24 | $3.43 \pm 0.62$ |
| | 94/067–94/074 | 2.60 | $3.63 \pm 0.94$ |
| | 94/109–94/116 | 2.89 | $3.92 \pm 0.89$ |
| | 94/137–94/144 | 2.01 | $4.63 \pm 1.76$ |
| | 94/213–94/216 | 0.91 | $< 4.78$ |
| | 96/081–96/094 | 0.84 | $3.20 \pm 1.94$ |

TABLE 1—*Continued*

| Object | $\Gamma^{b}$or Dates | Exposure[c] | Photon flux[d] |
|---|---|---|---|
| | Seyfert 2s | | |
| MCG –5-23-16 | $2.17^{+0.35}_{-0.41}$ | 7.72 | $4.26 \pm 0.55$ |
| | 92/219–92/224 | 1.77 | $4.53 \pm 1.02$ |
| | 92/241–92/245 | 1.07 | $4.32 \pm 1.33$ |
| | 94/216–94/221 | 0.56 | $4.12 \pm 2.41$ |
| | 94/263–94/277 | 4.32 | $4.15 \pm 0.77$ |
| Mkn 3 | $1.35^{+0.40}_{-0.94}$ | 9.65 | $1.87 \pm 0.51$ |
| | 94/074–94/081 | 3.12 | $1.59 \pm 0.87$ |
| | 94/213–94/216 | 1.06 | $< 3.02$ |
| | 95/045–95/052 | 2.62 | $2.71 \pm 0.98$ |
| | 95/052–95/059 | 2.85 | $3.19 \pm 0.94$ |
| NGC 1275 | — | 6.57 | $1.97 \pm 0.52$ |
| | 91/333–91/346 | 4.46 | $1.58 \pm 0.55$ |
| | 94/116–94/130 | 2.11 | $2.79 \pm 1.13$ |
| NGC 2110 | $2.04^{+0.43}_{-0.73}$ | 4.48 | $4.06 \pm 0.81$ |
| | 96/149–96/163 | 4.48 | $4.06 \pm 0.81$ |
| NGC 4388 | $2.00^{+0.13}_{-0.14}$ | 17.75 | $8.82 \pm 0.45$ |
| | 92/261–92/282 | 5.31 | $8.13 \pm 0.74$ |
| | 93/238–93/250 | 1.67 | $13.78 \pm 1.12$ |
| | 95/220–95/234 | 2.91 | $7.98 \pm 1.06$ |
| | 95/290–95/304 | 2.75 | $13.53 \pm 1.11$ |
| | 97/203–97/217 | 2.71 | $5.85 \pm 1.39$ |
| | 97/280–97/293 | 2.40 | $5.86 \pm 1.36$ |
| NGC 4507 | $1.74^{+0.23}_{-0.24}$ | 8.88 | $4.66 \pm 0.58$ |
| | 93/033–93/040 | 1.54 | $6.32 \pm 1.08$ |
| | 93/215–93/222 | 1.36 | $6.57 \pm 1.16$ |
| | 96/289–96/303 | 2.62 | $3.84 \pm 1.26$ |
| | 97/105–97/126 | 3.36 | $3.77 \pm 0.95$ |
| NGC 4945 | $2.11^{+0.21}_{-0.19}$ | 18.50 | $6.86 \pm 0.49$ |
| | 94/305–94/313 | 1.31 | $11.52 \pm 1.19$ |
| | 96/002–96/005 | 1.10 | $8.54 \pm 1.59$ |
| | 96/005–96/016 | 3.98 | $13.05 \pm 1.25$ |
| | 97/280–97/307 | 9.47 | $4.47 \pm 0.67$ |
| | 98/314–98/320 | 2.64 | $3.09 \pm 1.24$ |
| NGC 5506 | $2.85^{+0.35}_{-0.34}$ | 7.00 | $5.72 \pm 0.72$ |
| | 94/347–94/354 | 2.18 | $5.06 \pm 1.10$ |
| | 94/354–95/003 | 3.21 | $5.88 \pm 0.91$ |
| | 95/318–95/325 | 0.60 | $< 7.38$ |
| | 95/332–95/341 | 1.01 | $9.44 \pm 2.47$ |
| NGC 7172 | $2.18^{+0.27}_{-0.28}$ | 8.84 | $7.10 \pm 0.72$ |

Table 1—*Continued*

| Object | $\Gamma^{b}$or Dates | Exposure[c] | Photon flux[d] |
|---|---|---|---|
| | 95/053–95/059 | 1.37 | $4.47 \pm 1.62$ |
| | 95/059–95/066 | 1.42 | $4.71 \pm 1.35$ |
| | 95/066–95/080 | 2.20 | $9.12 \pm 1.11$ |
| | 96/038–96/044 | 2.68 | $8.42 \pm 1.37$ |
| | 97/161–97/168 | 1.18 | $6.25 \pm 3.04$ |
| NGC 7582 | — | 4.48 | $3.77 \pm 0.98$ |
| | 91/347–91/361 | 2.70 | $5.11 \pm 1.44$ |
| | 92/093–92/100 | 0.59 | $4.83 \pm 1.61$ |
| | 92/100–92/107 | 0.26 | $< 7.65$ |
| | 92/107–92/114 | 0.30 | $< 4.50$ |
| | 94/347–94/354 | 0.63 | $< 4.41$ |

[a]All uncertainties here are $1\sigma$; the first row for each object corresponds to sum of all its observations.

[b]The 50–200 keV photon index for objects with $\gtrsim 4\sigma$ detection.

[c]In units of $10^5$ s scaled to a single OSSE detector.

[d]For 50–150 keV in units of $10^{-4}$ cm$^{-2}$ s$^{-1}$.

Table 2

Spectral fits of the average OSSE spectra of Seyferts of type 1 and 2

| Model[a] | Type | $F^{b}$ | $\Gamma$ or $y^{c}$ | $E_{c}$ or $kT^{d}$ | $\chi^2_\nu$ |
|---|---|---|---|---|---|
| PL | 1 | 5.4 | $2.56^{+0.14}_{-0.14}$ | – | 30.9/35 |
| | 2 | 7.0 | $2.21^{+0.12}_{-0.12}$ | – | 30.5/27 |
| EPL | 1 | 5.5 | $1.69^{+0.57}_{-0.81}$ | $120^{+220}_{-60}$ | 23.8/34 |
| | 2 | 7.0 | $1.33^{+0.56}_{-0.52}$ | $130^{+220}_{-50}$ | 21.8/26 |
| TC | 1 | 5.4 | $0.89^{+0.36}_{-0.52}$ | $69^{+134}_{-28}$ | 24.1/34 |
| | 2 | 7.0 | $1.09^{+0.29}_{-0.41}$ | $84^{+101}_{-31}$ | 21.7/26 |

[a]The uncertainties correspond to 90% confidence of 1 parameter.

[b]Normalization given by the 50–150 keV flux in units of $10^{-11}$ erg cm$^{-2}$ s$^{-1}$.

[c]The photon index or the Compton parameter.

[d]The e-folding energy or temperature in keV.